

# $G_{Ep}/G_{Mp}$ ratio by polarization transfer in $\vec{e}p \rightarrow e\vec{p}$

M.K. Jones,<sup>1</sup> K.A. Aniol,<sup>7</sup> F.T. Baker,<sup>4</sup> J. Berthot,<sup>6</sup> P.Y. Bertin,<sup>6</sup> W. Bertozzi,<sup>22</sup> A. Besson,<sup>6</sup> L. Bimbot,<sup>26</sup> W.U. Boeglin,<sup>10</sup> E.J. Brash,<sup>5</sup> D. Brown,<sup>21</sup> J.R. Calarco,<sup>23</sup> L.S. Cardman,<sup>30</sup> C.-C. Chang,<sup>21</sup> J.-P. Chen,<sup>30</sup> E. Chudakov,<sup>30</sup> S. Churchwell,<sup>8</sup> E. Cisbani,<sup>15</sup> D.S. Dale,<sup>18</sup> R. De Leo,<sup>14</sup> A. Deur,<sup>6,30</sup> B. Diederich,<sup>25</sup> J.J. Domingo,<sup>30</sup> M.B. Epstein,<sup>7</sup> L.A. Ewell,<sup>21</sup> K.G. Fissum,<sup>22</sup> A. Fleck,<sup>5</sup> H. Fonvieille,<sup>6</sup> S. Frullani,<sup>15</sup> J. Gao,<sup>22</sup> F. Garibaldi,<sup>15</sup> A. Gasparian,<sup>13,18</sup> G. Gerstner,<sup>1</sup> S. Gilad,<sup>22</sup> R. Gilman,<sup>2,30</sup> A. Glamazdin,<sup>19</sup> C. Glashausser,<sup>2</sup> J. Gomez,<sup>30</sup> V. Gorbenko,<sup>19</sup> A. Green,<sup>33</sup> J.-O. Hansen,<sup>30</sup> C.R. Howell,<sup>8</sup> G.M. Huber,<sup>5</sup> M. Iodice,<sup>15</sup> C.W. de Jager,<sup>30</sup> S. Jaminion,<sup>6</sup> X. Jiang,<sup>2</sup> W. Kahl,<sup>28</sup> J.J. Kelly,<sup>21</sup> M. Khayat,<sup>17</sup> L.H. Kramer,<sup>10</sup> G. Kumbartzki,<sup>2</sup> M. Kuss,<sup>30</sup> E. Lakuriki,<sup>29</sup> G. Lavessière,<sup>6</sup> J.J. LeRose,<sup>30</sup> M. Liang,<sup>30</sup> R.A. Lindgren,<sup>32</sup> N. Liyanage,<sup>22</sup> G.J. Lolos,<sup>5</sup> R. Macri,<sup>8</sup> R. Madey,<sup>17</sup> S. Malov,<sup>2</sup> D.J. Margaziotis,<sup>7</sup> P. Markowitz,<sup>10</sup> K. McCormick,<sup>25</sup> J.I. McIntyre,<sup>2</sup> R.L.J. van der Meer,<sup>5</sup> R. Michaels,<sup>30</sup> B.D. Milbrath,<sup>9</sup> J.Y. Mougey,<sup>12</sup> S.K. Nanda,<sup>30</sup> E.A.J.M. Offermann,<sup>30</sup> Z. Papandreou,<sup>5</sup> C.F. Perdrisat,<sup>1</sup> G.G. Petratos,<sup>17</sup> N.M. Piskunov,<sup>16</sup> R.I. Pomatsalyuk,<sup>19</sup> D.L. Prout,<sup>17</sup> V. Punjabi,<sup>3</sup> G. Quéméner,<sup>1,12</sup> R.D. Ransome,<sup>2</sup> B.A. Raue,<sup>10</sup> Y. Roblin,<sup>6</sup> R. Roche,<sup>11</sup> G. Rutledge,<sup>1</sup> P.M. Rutt,<sup>30</sup> A. Saha,<sup>30</sup> T. Saito,<sup>31</sup> A.J. Sarty,<sup>11</sup> T.P. Smith,<sup>23</sup> P. Sorokin,<sup>19</sup> S. Strauch,<sup>2</sup> R. Suleiman,<sup>17</sup> K. Takahashi,<sup>31</sup> J.A. Templon,<sup>4</sup> L. Todor,<sup>25</sup> P.E. Ulmer,<sup>25</sup> G.M. Urciuoli,<sup>15</sup> P. Vernin,<sup>27</sup> B. Vlahovic,<sup>24</sup> H. Voskanyan,<sup>34</sup> K. Wijesooriya,<sup>1</sup> B.B. Wojtsekowski,<sup>30</sup> R.J. Woo,<sup>20</sup> F. Xiong,<sup>22</sup> G.D. Zainea,<sup>5</sup> and Z.-L. Zhou<sup>22</sup>

(*The Jefferson Lab Hall A Collaboration*)

<sup>1</sup>College of William and Mary, Williamsburg, VA 23187

<sup>2</sup>Rutgers, The State University of New Jersey, Piscataway, NJ 08855

<sup>3</sup>Norfolk State University, Norfolk, VA 23504

<sup>4</sup>University of Georgia, Athens, GA 30602

<sup>5</sup>University of Regina, Regina, SK S4S 0A2, Canada

<sup>6</sup>Université Blaise Pascal/CNRS-IN2P3, F-63177 Aubière, France

<sup>7</sup>California State University at Los Angeles, Los Angeles, CA 90032

<sup>8</sup>Duke University and TUNL, Durham, NC 27708

<sup>9</sup>Eastern Kentucky University, Richmond, KY 40475

<sup>10</sup>Florida International University, Miami, FL 33199

<sup>11</sup>Florida State University, Tallahassee, FL 32306

<sup>12</sup>Institut des Sciences Nucléaires, CNRS-IN2P3, F-38026 Grenoble, France

<sup>13</sup>Hampton University, Hampton, VA 23668

<sup>14</sup>INFN, Sezione di Bari and University of Bari, 70126 Bari, Italy

<sup>15</sup>INFN, Sezione Sanità and Istituto Superiore di Sanità, 00161 Rome, Italy

<sup>16</sup>JINR-LHE, 141980 Dubna, Moscow Region, Russian Federation

<sup>17</sup>Kent State University, Kent, OH 44242

<sup>18</sup>University of Kentucky, Lexington, KY 40506

<sup>19</sup>Kharkov Institute of Physics and Technology, Kharkov 310108, Ukraine

<sup>20</sup>University of Manitoba, Winnipeg, MB R3T 2N2

<sup>21</sup>University of Maryland, College Park, MD 20742

<sup>22</sup>Massachusetts Institute of Technology, Cambridge, MA 02139

<sup>23</sup>University of New Hampshire, Durham, NH 03824

<sup>24</sup>North Carolina Central University, Durham, NC 27707

<sup>25</sup>Old Dominion University, Norfolk, VA 23508

<sup>26</sup>Institut de Physique Nucléaire, F-91406 Orsay, France

<sup>27</sup>CEA Saclay, F-91191 Gif-sur-Yvette, France

<sup>28</sup>Syracuse University, Syracuse, NY 13244

<sup>29</sup>Temple University, Philadelphia, PA 19122

<sup>30</sup>Thomas Jefferson National Accelerator Facility, Newport News, VA 23606

<sup>31</sup>Tohoku University, Sendai 980, Japan

<sup>32</sup>University of Virginia, Charlottesville, VA 22901

<sup>33</sup>Western Cape University, Capetown, South Africa

<sup>34</sup>Yerevan Physics Institute, Yerevan 375036, Armenia

(October 14, 2018)

The ratio of the proton's elastic electromagnetic form factors  $G_{Ep}/G_{Mp}$  was obtained by measuring  $P_t$  and  $P_\ell$ , the

transverse and longitudinal recoil proton polarization, respectively. For elastic  $\vec{e}p \rightarrow e\vec{p}$ ,  $G_{Ep}/G_{Mp}$  is proportional to

$P_t/P_\ell$ . The four-momentum transfer squared,  $Q^2$ , was between 0.5 and 3.5  $\text{GeV}^2$ . Simultaneous measurement of  $P_t$  and  $P_\ell$  in a polarimeter provides good control of the systematic uncertainty. The results for the ratio  $G_{Ep}/G_{Mp}$  show a systematic decrease with increasing  $Q^2$ , indicating for the first time a marked difference in the spatial distribution of charge and magnetization currents in the proton.

25.30.Bf, 13.40.Gp, 24.85.+p

The nucleon electromagnetic form factors are directly connected to the spatial distribution of the charge and current inside the proton and neutron, and hence intimately related to their internal structure. The high energy, current and polarization, unique to the Continuous Electron Beam Accelerator Facility of the Jefferson Laboratory (JLab), make it possible to investigate the internal structure of the nucleon with higher precision and different experimental techniques.

The earliest investigations of the proton form factor by Hofstadter *et al.* [1] established the dominance of the one-photon exchange process in the elastic  $ep$  reaction and indicated that  $F_{1p}$  and  $F_{2p}$ , the Dirac and Pauli form factors, have approximately the same  $Q^2$  dependence up to  $Q^2 \approx 0.5 \text{ GeV}^2$ . The data were fitted with a dipole shape,  $G_D = (1 + \frac{Q^2}{0.71})^{-2}$ , characteristic of an exponential charge distribution.

The elastic  $ep$  cross section can be written in terms of the Sachs form factors  $G_{Ep}$  (electric) and  $G_{Mp}$  (magnetic), which are defined in terms of  $F_{1p}$  and  $F_{2p}$  as:

$$G_{Ep} = F_{1p} - \tau \kappa_p F_{2p} \quad \text{and} \quad G_{Mp} = F_{1p} + \kappa_p F_{2p}, \quad (1)$$

where  $\tau = Q^2/4M^2$ ,  $\kappa_p$  is the anomalous nucleon magnetic moment and  $M$  the mass of the proton. In the limit  $Q^2 \rightarrow 0$ ,  $G_{Ep} = 1$  and  $G_{Mp} = \mu_p$ , the proton magnetic moment. The unpolarized  $ep$  cross section is:

$$\frac{d\sigma}{d\Omega} = \frac{\alpha^2 E'_e \cos^2 \frac{\theta_e}{2}}{4E_e^3 \sin^4 \frac{\theta_e}{2}} \left[ G_{Ep}^2 + \frac{\tau}{\epsilon} G_{Mp}^2 \right] \left( \frac{1}{1 + \tau} \right), \quad (2)$$

where  $E'_e$  and  $\theta_e$  are the scattered electron's energy and angle,  $E_e$  is the incident beam energy and  $\epsilon$  is the virtual photon longitudinal polarization,  $\epsilon = [1 + 2(1 + \tau) \tan^2(\frac{\theta_e}{2})]^{-1}$ .

In the Rosenbluth method [2], the separation of  $G_{Ep}^2$  and  $G_{Mp}^2$  is achieved by measuring the cross section at a given  $Q^2$  over a range of  $\epsilon$ -values that are obtained by changing the beam energy and scattered electron angle. In Eq. (2) the  $G_{Mp}$  part of the cross section is multiplied by  $\tau$ ; therefore, as  $Q^2$  increases, the cross section is dominated by  $G_{Mp}$ , making the extraction of  $G_{Ep}$  more difficult. Fig. 1 shows measurements of proton form factors obtained using this method. For  $Q^2 < 1 \text{ GeV}^2$ , the uncertainties in both  $G_{Ep}$  and  $G_{Mp}$  are only a few percent and one finds that  $G_{Mp}/\mu_p G_D \simeq G_{Ep}/G_D \simeq 1$ .

For  $G_{Ep}$  above  $Q^2 = 1 \text{ GeV}^2$ , the large uncertainties and the divergence in results between different experiments, as seen in Fig. 1a, illustrate the difficulties in obtaining  $G_{Ep}$  by the Rosenbluth method. In contrast, the uncertainties on  $G_{Mp}$  remain small up to  $Q^2 = 31.2 \text{ GeV}^2$  [10].

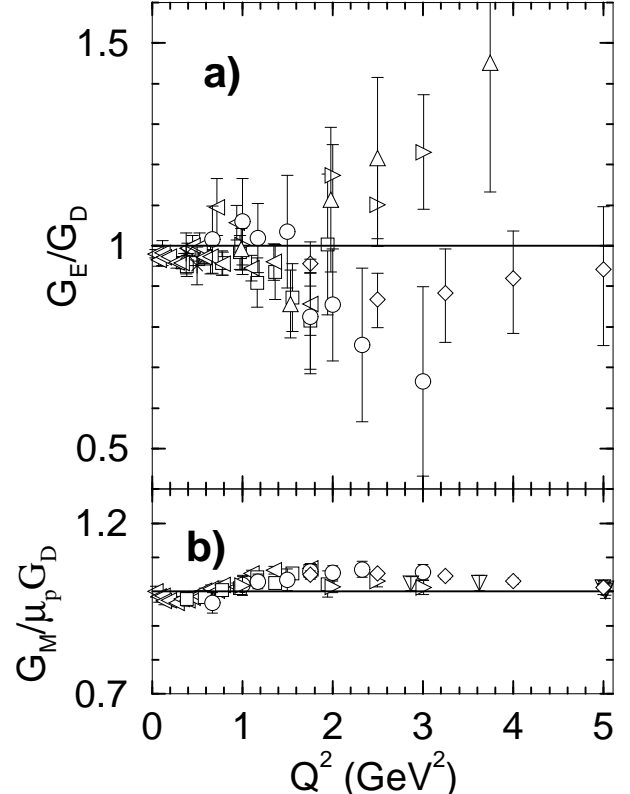


FIG. 1. World data for (a)  $G_{Ep}/G_D$  and (b)  $G_{Mp}/\mu_p G_D$ . Refs. [3]△, [4]□, [5]◀, [6]○, [7]▷, [8]◇, [9]\*, and [10]▽, versus  $Q^2$ .

This experiment used the powerful technique of polarization transfer, resulting in small systematic uncertainties. For one-photon exchange, the scattering of longitudinally polarized electrons results in a transfer of polarization to the recoil proton with two in-scattering-plane components,  $P_t$  perpendicular to and  $P_\ell$  parallel to the proton momentum, given by [11]:

$$I_0 P_t = -2\sqrt{\tau(1 + \tau)} G_{Ep} G_{Mp} \tan \frac{\theta_e}{2}, \quad (3)$$

$$I_0 P_\ell = \frac{1}{M} (E_e + E'_e) \sqrt{\tau(1 + \tau)} G_{Mp}^2 \tan^2 \frac{\theta_e}{2}, \quad (4)$$

where

$$I_0 = G_{Ep}^2(Q^2) + \tau G_{Mp}^2(Q^2) [1 + 2(1 + \tau) \tan^2 \frac{\theta_e}{2}]. \quad (5)$$

Equations (3) and (4) together give:

$$\frac{G_{Ep}}{G_{Mp}} = -\frac{P_t}{P_\ell} \frac{(E_e + E'_e)}{2M} \tan \left( \frac{\theta_e}{2} \right). \quad (6)$$

The ratio  $G_{Ep}/G_{Mp}$  can be obtained from a simultaneous measurement of the two recoil polarization components in the polarimeter; neither the beam polarization nor the polarimeter analyzing power needs to be known. This method was first used by Milbrath *et al.* [9] at M.I.T.-Bates to measure the ratio  $G_{Ep}/G_{Mp}$  at low  $Q^2$ .

Our experiment was done in Hall A at JLab. Longitudinally polarized electron beams with energies between 0.934 GeV and 4.090 GeV were scattered in a 15 cm long, circulating liquid hydrogen ( $LH_2$ ) target, refrigerated to 19 K. The kinematics settings are in Table I. For the four highest  $Q^2$  points, a bulk GaAs photo-cathode excited by circularly polarized laser light produced beams with  $\sim 0.39$  polarization and currents up to  $\sim 115 \mu A$ ; the helicity was flipped at 30 Hz. For the lower  $Q^2$  points, a strained GaAs crystal was used, and typical polarizations of  $\sim 0.60$  were achieved with currents up to  $\sim 15 \mu A$ ; the helicity was flipped at 1 Hz. The beam polarization was measured with a Mott polarimeter in the injector line and with a Møller polarimeter in Hall A.

Elastic  $ep$  events were selected by detecting the scattered electrons and protons in coincidence in the two identical High Resolution Spectrometers (HRS) of Hall A [12]. The HRS's deflect particles vertically by  $45^\circ$  and accept a maximum central trajectory momentum of 4 GeV/c with a 6.5 msr angular acceptance,  $\pm 5\%$  momentum acceptance and  $\sim 10^{-4}$  momentum resolution. A schematic of the hadron detector stack is shown in Fig. 2.

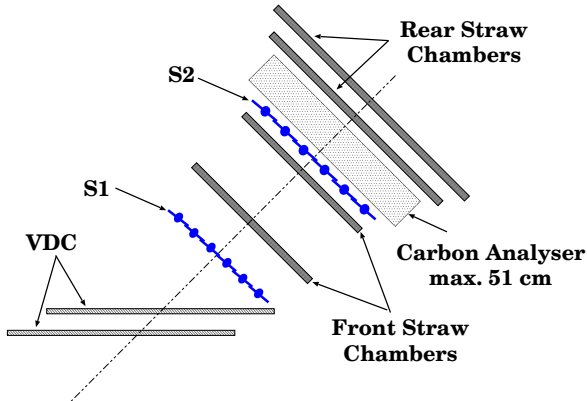


FIG. 2. Schematic of hadron detector stack .

The two vertical drift chambers (VDC) installed close to the focal plane of each HRS define position and angle with high precision. The trigger was defined by a coincidence between the signals from scintillator planes  $S_1$  and  $S_2$  in the two HRS's. A focal plane polarimeter (FPP) was built and installed in the hadron HRS by a collaboration of Rutgers University, the College of William and Mary, Norfolk State University, the University of Georgia, and the University of Regina. In the FPP, two front straw chambers are located between  $S_1$  and  $S_2$  and define the incident proton trajectory [13]. The protons are

scattered in the graphite analyzer located after  $S_2$ . The two rear straw chambers define the proton trajectory after scattering in the graphite. The active areas of the first two chambers are  $60 \times 209 \text{ cm}^2$ , chambers 3 and 4 are  $124 \times 272 \text{ cm}^2$  and  $142 \times 295 \text{ cm}^2$ , respectively. The spatial resolution of the straws is about  $250 \mu\text{m}$ . The graphite analyzer consists of 5 sets of graphite plates that can be moved out to collect straight-through trajectories for alignment of the FPP chambers. To optimize the FPP figure of merit, different graphite thicknesses were used: 11.4 and 22.9 cm for  $Q^2=0.5$  and 0.8 GeV $^2$ , respectively; 41.9 cm for both 1.2 and 1.5 GeV $^2$ , and 49.5 cm for all larger  $Q^2$ -values. The graphite density is  $1.70 \text{ g/cm}^3$ .

The azimuthal angular distribution after a second scattering in the analyzer of the FPP is given by:

$$N_p(\theta, \varphi) = N_p(\theta) \left( 1 + h A_c(\theta) \left[ P_t^{fpp} \sin \varphi - P_n^{fpp} \cos \varphi \right] \right), \quad (7)$$

where  $h$  is the electron beam polarization,  $N_p(\theta)$  is the number of protons scattered in the polarimeter,  $\theta$  and  $\varphi$  are the polar and azimuthal angles after scattering, and  $A_c(\theta)$  is the analyzing power;  $P_t^{fpp}$  and  $P_n^{fpp}$  are the in-plane polarization components, transverse and normal, respectively, at the FPP analyzer. Instrumental asymmetries are canceled by taking the difference of the azimuthal distributions for positive and negative electron beam helicity. Fourier analysis of this difference distribution gives the two physical amplitudes in Eq. (7).

The proton spin precesses in the fields of the magnetic elements of the HRS, and therefore the polarizations at the target and the FPP are different; they are related through a spin transport matrix  $\mathbf{P}^{fpp} = (\mathbf{S}) \times \mathbf{P}$ , where  $\mathbf{P}^{fpp}$  and  $\mathbf{P}$  are polarization column vectors  $(n, t, \ell)$  at the FPP and target, respectively, and  $(\mathbf{S})$  is the spin transport matrix. A novel method was developed to extract the values of the polarization components  $P_t$  and  $P_\ell$  at the target from the FPP azimuthal distribution; the integrals in the Fourier analysis were replaced with sums weighted by the values of the matrix elements,  $S_{ij}$ , of each event [14]. The matrix elements  $S_{ij}$  depend upon the scattering angles ( $\theta$  and  $\phi$ ), spatial coordinate ( $y$ ) at the target and proton momentum ( $p$ ). The  $S_{ij}$ 's were calculated for each event from the measured  $y, \phi, \theta, p$  using the spin matrix determined by a magnetic transport code. Both the ray-tracing code SNAKE [15] and the differential-algebra-based code COSY [16] were used, and the spin precession corrections from both methods agree within experimental uncertainties. The stability of the method was studied in detail for all  $Q^2$ . The data were analyzed in bins of each one of the four target variables, one at a time. The results showed that the extracted  $G_{Ep}/G_{Mp}$  ratio is independent of each of these variables.

The results for the ratio  $\mu_p G_{Ep}/G_{Mp}$  are shown with filled circles in Fig. 3a, and as the ratio  $Q^2 F_2/F_1$ , obtained from Eq. (1), in Fig. 3b; in both figures only the

statistical uncertainties are shown. The data are tabulated in Table I, where both statistical ( $\sigma_{stat}$ ) and systematic ( $\sigma_{sys}$ ) uncertainties are given for each data point. Three sources contribute to this systematic uncertainty: measurement of the target variables, positioning and field strength of the HRS magnetic elements, and uncertainties in the dipole fringe field characterization. The systematic uncertainties would shift all data points in the same direction, either up or down. No radiative correction has been applied to the results. External radiative effects are canceled by switching the beam helicity. The internal correction is due to hard photon emission, two-photon exchange and higher-order contributions. A dedicated calculation [17] predicts the first to be of the order of a few per cent. Preliminary indications are that the two other contributions are also at the same percentage level.

The most important feature of the data is the sharp decline of the ratio  $\mu_p G_{Ep}/G_{Mp}$  as  $Q^2$  increases, which indicates that  $G_{Ep}$  falls faster than  $G_{Mp}$ . Furthermore, as  $G_{Mp}/\mu_p G_D$  is approximately constant, it follows that  $G_{Ep}$  falls more rapidly with  $Q^2$  than the dipole form factor  $G_D$ .

Results from this experiment are consistent with the earlier results of refs. [4,5,6] which have much larger uncertainties. Our results are compatible with the SLAC data of ref. [8] up to about  $Q^2$  of 2.5 GeV $^2$ , considering the larger uncertainties, but our results are in definite disagreement with the older results of ref. [7] from SLAC, as seen in Fig. 3b.

The  $Q^2 F_2/F_1$  ratio shown in Fig. 3b indicates a continuing increase with  $Q^2$ , contradicting earlier observations based on the data of refs. [7,8] that it might have reached a constant value as predicted in pQCD:  $F_1 \sim \frac{1}{Q^2}$  and  $F_2 \sim \frac{1}{Q^4}$ . It would be of great interest to explore the larger  $Q^2$  region where pQCD will dominate. Extension of this experiment to larger  $Q^2$  has become a very interesting prospect and is planned in the near future.

TABLE I. The ratios  $\mu_p G_{Ep}/G_{Mp}$  from this experiment.

$\langle Q^2 \rangle$	$E_e$	$\theta_p$	$\mu_p G_{Ep}/G_{Mp}$	$\sigma_{stat}$	$\sigma_{sys}$
GeV $^2$	GeV	degrees			
0.49	0.934	45.3	0.966	0.022	0.011
0.79	0.934	30.8	0.950	0.015	0.017
1.18	1.821	40.4	0.869	0.014	0.027
1.48	3.395	46.5	0.798	0.033	0.035
1.77	3.395	42.9	0.728	0.026	0.047
1.88	4.087	43.4	0.720	0.031	0.060
2.47	4.090	37.7	0.726	0.027	0.062
2.97	4.087	33.6	0.612	0.032	0.056
3.47	4.090	29.9	0.609	0.047	0.045

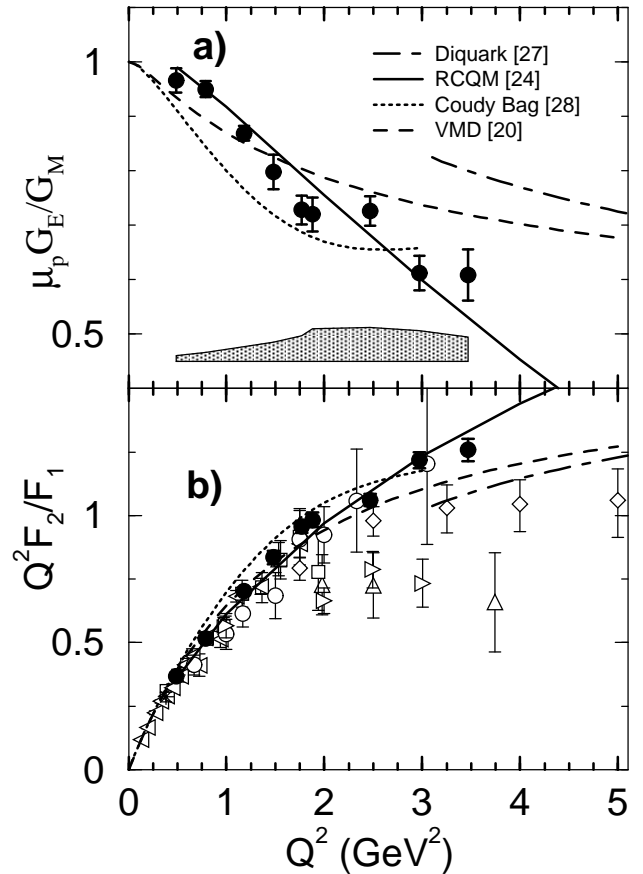


FIG. 3. (a) The ratio  $\mu_p G_{Ep}/G_{Mp}$  from this experiment, compared with theoretical calculations; the absolute value of  $\sigma_{sys}$  is shown by the shaded area. (b) The ratio  $Q^2 F_2/F_1$  for the same data, compared to the same theoretical models as in 3a and world data; symbols as in Fig. 1.

The fundamental understanding of the nucleon form factors in terms of QCD is one of the outstanding problems in nuclear physics. So far all theoretical models of the nucleon form factors are based on effective theories; they all rely on a comparison with existing data and their parameters are adjusted to the data. Much work has been done with the goal of bridging the low and high  $Q^2$  regimes. There are two quite different approaches to calculate nucleon form factors. In the first kind, the mesonic degrees of freedom are explicit, as in dispersion relation calculations based on Vector Meson Dominance [18,19,20,21], models comprising a three-quark core dressed with pseudoscalar mesons [22], and a calculation based on the solitonic nature of the nucleon [23]. The second kind are QCD-based quark models; these include models such as relativistic constituent quark (RCQM) [24,25,26,27], diquark [28], cloudy bag [29], skewed parton distribution (SPD) [30,31,32], and QCD sum rule [33]. Calculations of the nucleon form factors from lattice QCD are in progress [34]. In Fig. 3 we show as a dashed curve the ratios of  $\mu_p G_{Ep}/G_{Mp}$  and  $Q^2 F_2/F_1$  calculated from the latest published fit

to the proton and neutron form factors of Mergell *et al.* [21] based on VMD (not including data from this experiment). These authors use dispersion relations for the form factors, with spectral functions taking into account the dominant vector meson poles as well as the two-pion channel; an asymptotic behavior consistent with pQCD was also included.

In the earliest study of the RCQM, Chung and Coester [24] investigated the effect of the constituent quark masses, the anomalous magnetic moment of the quarks,  $F_{2q}$ , and the confinement scale parameter. Recently Coester introduced a form factor for  $F_{2q}$  to reproduce the present data; the result is the solid curve in Fig. 3 [25]. This demonstrates how the new  $G_{Ep}/G_{Mp}$  data can help constrain the basic inputs to a particular model.

The dashed-dot curve in Fig. 3 shows the recently re-evaluated di-quark model prediction of Kroll *et al.* [28]. In the limit  $Q^2 \rightarrow \infty$  this model is equivalent to the hard-scattering formulation of pQCD. Calculations based on the cloudy bag model predict the right slope for  $G_{Ep}/G_{Mp}$ , shown as a dotted curve in Fig. 3; this model includes an elementary pion field coupled to the quarks inside the bag such that chiral symmetry is restored [29].

Recent theoretical developments indicate that measurements of the elastic form factors of the proton to large  $Q^2$  may shed light on the problem of nucleon spin. This connection between elastic form factors and spin has been demonstrated within the SPD formalism by Ji [30]. The first moment of the SPD taken in the forward limit yields, according to the Angular Momentum Sum Rule [30], a contribution to the nucleon spin from the quarks and gluons, including the orbital angular momentum. By subsequently applying the Sum Rule to the SPD, it should become possible to estimate the total contribution of the valence quarks to the proton spin.

To conclude, we have presented a new measurement of  $G_{Ep}/G_{Mp}$  obtained in a polarization transfer experiment with unprecedented accuracy. The results demonstrate for the first time that the  $Q^2$  dependence of  $G_{Ep}$  and  $G_{Mp}$  is significantly different. The quality of the JLab data will place a tight constraint on the theoretical models. Results from this experiment combined with future measurements of the neutron form factors will bring us closer to a single description of the structure of the nucleon.

The collaboration thanks the Hall A technical staff and the Jefferson Lab Accelerator Division for their outstanding support during this experiment. This work was supported in part by the U.S. Department of Energy, the U.S. National Science Foundation, the Italian Institute for Nuclear Research, the French Commissariat à l'Energie Atomique and Centre National de la Recherche Scientifique (CNRS), and the Natural Sciences and Engineering Research Council of Canada.

---

- [1] R. Hofstadter and R.W. McAllister, Phys. Rev. **98**, 217 (1955); E.E. Chambers and R. Hofstadter, Phys. Rev. **103**, 1454 (1956).
- [2] M.N. Rosenbluth, Phys. Rev. **79**, 615 (1950).
- [3] J. Litt *et al.*, Phys. Lett. B **31**, 40 (1970).
- [4] Ch. Berger *et al.*, Phys. Lett. B **35**, 87 (1971).
- [5] L.E. Price *et al.*, Phys. Rev. D **4**, 45 (1971).
- [6] W. Bartel *et al.*, Nuc. Phys. B **58**, 429 (1973).
- [7] R.C. Walker *et al.*, Phys. Rev. D **49**, 5671 (1994); R.C. Walker *et al.*, Phys. Lett. B **224**, 353 (1989).
- [8] L. Andivahis *et al.*, Phys. Rev. D **50**, 5491 (1994); P.E. Bosted *et al.*, Phys. Rev. Lett. **68**, 3841 (1992).
- [9] B. Milbrath *et al.*, Phys. Rev. Lett. **80**, 452 (1998); erratum, Phys. Rev. Lett. **82**, 2221 (1999).
- [10] R. Arnold *et al.*, Phys. Rev. Lett. **57**, 174 (1986); A.F. Sill *et al.*, Phys. Rev. D **48**, 29 (1993).
- [11] A.I. Akhiezer and M.P. Rekalo, Sov. J. Part. Nucl. **3**, 277 (1974); R. Arnold, C. Carlson and F. Gross, Phys. Rev. C **23**, 363 (1981).
- [12] <http://www.jlab.org/Hall-A/equipment/>
- [13] M.K. Jones *et al.*, AIP Conf. Proc. **412**, ed. T.W. Donnelly, p.342 (1997). [http://www.jlab.org/Hall-A/equipment/detectors/fpp\\_overview.html](http://www.jlab.org/Hall-A/equipment/detectors/fpp_overview.html)
- [14] G. Quéméner *et al.*, to be pub. in Proceedings of the Int. Conf. on Nucl. Phys., INPC98, Paris (1998).
- [15] P. Vernin, SNAKE, private communication, SPhN-CEA in Saclay, France.
- [16] M. Bertz, COSY INFINITY version 7, NSCL Tech. Rep., MSUCL-977, Michigan State University (1995).
- [17] A.V. Afanasev, I. Akushevich, and N. Merenkov, private communication (1999).
- [18] G. Höhler *et al.*, Nucl. Phys. B **114**, 505 (1976).
- [19] F. Iachello, A.D. Jackson, and A. Landé, Phys. Lett. B **43**, 191 (1973).
- [20] M.F. Gari and W. Krümpelmann, Z. Phys. A **322**, 689 (1985) .
- [21] P. Mergell, U.G. Meissner, and D. Drechsel, Nucl. Phys. A **596**, 367 (1996).
- [22] Z. Dziembowski *et al.*, Ann. of Phys. **258**, 1 (1997).
- [23] G. Holzwarth, Z. Phys. A **356**, 339 (1996).
- [24] P.L. Chung and F. Coester, Phys. Rev. D **44**, 229 (1991).
- [25] F. Coester, private communication (1999).
- [26] I.G. Aznauryan, Phys. Lett. B **316**, 391 (1993).
- [27] M.R. Frank, B.K. Jennings, and G.A. Miller, Phys. Rev. C **54**, 920 (1996).
- [28] P. Kroll, M. Schürmann, and W. Schweiger, Z. Phys. A **338**, 339 (1991); private communication (1998).
- [29] D.H. Lu, A.W. Thomas, and A.G. Williams, Phys. Rev. C **57**, 2628 (1998); D.H. Lu, S.N. Yang and A.W. Thomas, preprint ADP 99-36/t373.
- [30] X. Ji, Phys. Rev. D **55**, (1997) 7114; Phys. Rev. Lett. **78**, 610 (1997).
- [31] A.V. Radyushkin, JLab-THY-98-10 and hep-ph/9803316.
- [32] A.V. Afanasev, hep-ph/9808291 V2 and private communication (1999).
- [33] A.V. Radyushkin, Acta Phys. Pol. B **15**, 40 (1984).

[34] S. Capitani et al. , hep-lat/9809172; *Lattice '98*, Proc. of the Int. Symp., ed. by T. DeGrand *et al.*, Boulder, CO, 1998, Nucl. Phys. B (Proc. Suppl.), (1998).